Research in Pharmaceutical Sciences, June 2025; 20(3): 445-455
Received: 03-08-2024
Peer Reviewed: 22-09-2024
Revised: 16-10-2024
Accepted: 04-05-2025
Published: 17-06-2025

School of Pharmacy & Pharmaceutical Sciences
Isfahan University of Medical Sciences

Original Article

Synthesis of thiosemicarbazone derivatives and evaluation of their cytotoxicity with emphasis on ferroptosis biomarkers; an *in vitro* study

Yasaman Shadmani[1], Yaghoub Pourshojaei[2,3,*], Somayyeh Karami-Mohajeri[1,4,*], Bagher Amirheidari[3,5], and Motahareh Sadeghzadeh[2]

[1]*Department of Toxicology and Pharmacology, Faculty of Pharmacy, Kerman University of Medical Sciences, Kerman, Iran.*
[2]*Department of Medicinal Chemistry, Faculty of Pharmacy, Kerman University of Medical Sciences, Kerman, Iran.*
[3]*Extremophile and Productive Microorganisms Research Center, Kerman University of Medical Sciences, Kerman, Iran.*
[4]*Pharmaceutics Research Center, Institute of Neuropharmacology, Kerman University of Medical, Kerman, Iran.*
[5]*Department of Pharmaceutical Biotechnology, Faculty of Pharmacy, Kerman University of Medical Sciences, Kerman, Iran.*

Abstract

Background and purpose: This study aimed to evaluate the cytotoxicity of synthesized thiosemicarbazone derivatives, particularly on biomarkers associated with ferroptosis.
Experimental approach: Thiosemicarbazone derivatives (C1-C5) were synthesized by condensation between thiosemicarbazide and the corresponding benzaldehyde derivatives. The compounds were characterized using IR spectroscopy and H/C NMR spectroscopy. To evaluate their biological activity, PC-12 cells were cultured in DMEM/MEM medium supplemented with 10% bovine serum albumin. Cell viability was assessed using the MTT assay, while intracellular reactive oxygen species (ROS) levels were measured using DCFH-DA. Additionally, glutathione peroxidase (GPX) activity, lipid peroxidation (LPO), and total antioxidant capacity (TAC) were evaluated to determine oxidative stress and antioxidant response.
Findings/Results: In cell viability assessments, C2 exhibited the highest toxicity, while C4 demonstrated the lowest toxicity after 24 h. Among all derivatives, only C3 reduced ROS levels without affecting GPX activity. All derivatives effectively reduced LPO, although C5 showed the least effectiveness in this regard. In contrast to C2 and C5, TAC was significantly higher than the control after treatment with C1, C3, and C4.
Conclusion and implications: These findings suggest that thiosemicarbazone derivatives may influence the ferroptosis cell death pathway through their chelation properties, necessitating further research on their ability to bind to iron. Their effects on oxidative stress and cellular antioxidant capacity provide valuable insights for therapeutic strategies.

Keywords: Antioxidant capacity; Cytotoxicity; Ferroptosis; Iron chelators; Lipid peroxidation; Thiosemicarbazones.

INTRODUCTION

Cell death is an essential biological process that occurs in all living organisms, influenced by factors such as embryogenesis, development, tissue turnover, and responses to external stimuli (1,2). Since the 1960s and 70s, researchers have conducted systematic studies to understand cell death pathways (3,4). These pathways can be categorized into accidental and regulated forms, including programmed cell death, which encompasses a variety of mechanisms (5). When cells encounter irreparable damage from internal errors or external toxins, several cell death programs are activated, including apoptosis, autophagy, necrosis, and newer forms like ferroptosis (6).

*Corresponding authors:
S. Karami-Mohajeri, Tel: +98-3431325001, Fax: +98-3431325003
Email: s_karami@kmu.ac.ir, somayyehkarami@gmail.com
Y. Pourshojaei, Tel: +98-3431325001, Fax: +98-3431325003
Email: y.pourshoja@kmu.ac.ir, pourshojaei@yahoo.com

Access this article online

Website: http://rps.mui.ac.ir

DOI: 10.4103/RPS.RPS_120_24

Ferroptosis, a term introduced by Brent Stockwell in 2012, describes a distinct type of cell death characterized by iron-dependent lipid peroxidation (LPO). This process is critical in various biological contexts, including development, immunity, aging, and cancer (7). While inhibition of ferroptosis is linked to tumor development, excessive ferroptosis is associated with neurodegenerative diseases and organ injuries (8-10). Recent research highlights ferroptosis's role in the pathogenesis of cardiovascular diseases and neurodegenerative diseases (11,12).

Key factors driving ferroptosis include the peroxidation of polyunsaturated fatty acids (PUFAs), accumulation of Fe^{2+} ions, dysfunction of glutathione peroxidase 4 (GPX4), and depletion of intracellular glutathione (GSH) (13,14). The peroxidation of PUFAs leads to cellular and mitochondrial membrane damage, ultimately triggering ferroptotic cell death (15,16). Under normal conditions, GPX4 reduces lipid peroxides to alcohols through GSH oxidation, thereby protecting against ferroptosis (17). However, GPX4 inactivation or GSH depletion can initiate LPO (18). The accumulation of iron and PUFAs, alongside a decrease in endogenous inhibitors such as GPX4, NADPH, GSH, and vitamin E, can induce ferroptosis (19-21). While iron is vital for many biological processes, its accumulation can lead to oxidative stress and cellular toxicity, particularly through Fenton reaction-mediated production of reactive oxygen species (ROS) and activation of iron-containing enzymes (22-25).

Ferroptosis inhibitors, including iron chelators and lipophilic radical-trapping antioxidants (*e.g.* ferrostatin-1 and liproxstatin-1), can prevent PUFAs peroxidation and may serve as therapeutic agents for conditions such as cardiovascular diseases and neurodegenerative diseases (26-28). Various iron chelators like deferoxamine, deferiprone, and deferasirox are used clinically to manage diseases associated with excessive iron accumulation by enhancing iron excretion and reducing tissue iron levels (24,29). Additionally, thiosemicarbazones are notable for their iron-chelating properties, inhibiting ribonucleotide reductase, an enzyme crucial for nucleotide synthesis that requires iron as a cofactor (19,30).

Thiosemicarbazones have gained attention in medicinal chemistry for their broad biological activities, including antineoplastic, antimicrobial, and antiviral properties (31-33). Given their potential as iron chelators, this study focuses on synthesizing thiosemicarbazone derivatives and evaluating their cytotoxic effects, particularly concerning biomarkers of ferroptosis.

MATERIALS AND METHODS

Chemistry

All raw chemicals, reagents, and solvents were commercially available and were used without further purification. An electrothermal IA9100 melting point apparatus fixed at 1 °C/min was used to determine the melting point. The infrared (IR) spectra were recorded on an FT-IR Tensor 27 infrared spectrophotometer (Bruker, Germany) using KBr as a matrix. Proton nuclear magnetic resonance (1H-NMR) and carbon-13 nuclear magnetic resonance (13C-NMR) spectra were taken by an FT-NMR Bruker Avance ultra shield spectrometer (300 and 75 MHz in frequencies for 1H and 13C, respectively) using DMSO-d_6 as solvent. Also, thin-layer chromatography (TLC)-grade silica gel G/UV 254 nm plates were used for monitoring reaction progress by the use of EtOAc/n-hexane (1:2 volume ratio) as eluent.

General procedures for the synthesis of the thiosemicarbazone compounds

Thiosemicarbazone derivatives (C1-C5) were synthesized *via* a condensation reaction between thiosemicarbazide and the appropriate benzaldehyde derivatives. In a 50 mL round-bottom flask equipped with a magnetic stir bar, a mixture of 10 mL of ethanol, 1 mmol of benzaldehyde derivatives A, and 1 mmol of thiosemicarbazide B was prepared. Then, 0.2 g of potassium carbonate was added to this mixture and stirred overnight at room temperature, followed by refluxing for 1 h. The reaction progress was monitored using TLC with an eluent of EtOAc/n-hexane (1:4). After

the reaction was complete, a solution of 20 mL of water and ice was added to the flask, leading to the precipitation of the desired compounds. The precipitate was then filtered, recrystallized, and dried, and its melting point was determined (34). The structure of the compounds was confirmed through IR and NMR analysis (Fig. 1).

Cell culture

PC12 cells were obtained from the Pasteur Institute of Iran and cultured in Dulbecco's Modified Eagle Medium (DMEM)/MEM (Gibco, USA), supplemented with 10% fetal bovine serum (FBS) and 1% penicillin-streptomycin (Gibco, USA) under sterile conditions. The cells were maintained in T-75 flasks in a humidified incubator at 37 °C with 5% CO_2. Once the cells reached 70-80% confluency, they were passaged using 0.25% trypsin-EDTA solution (Gibco, USA). After detachment, the cells were centrifuged at 1200 rpm for 5 min, resuspended in fresh medium, and plated at the appropriate density for subsequent experiments.

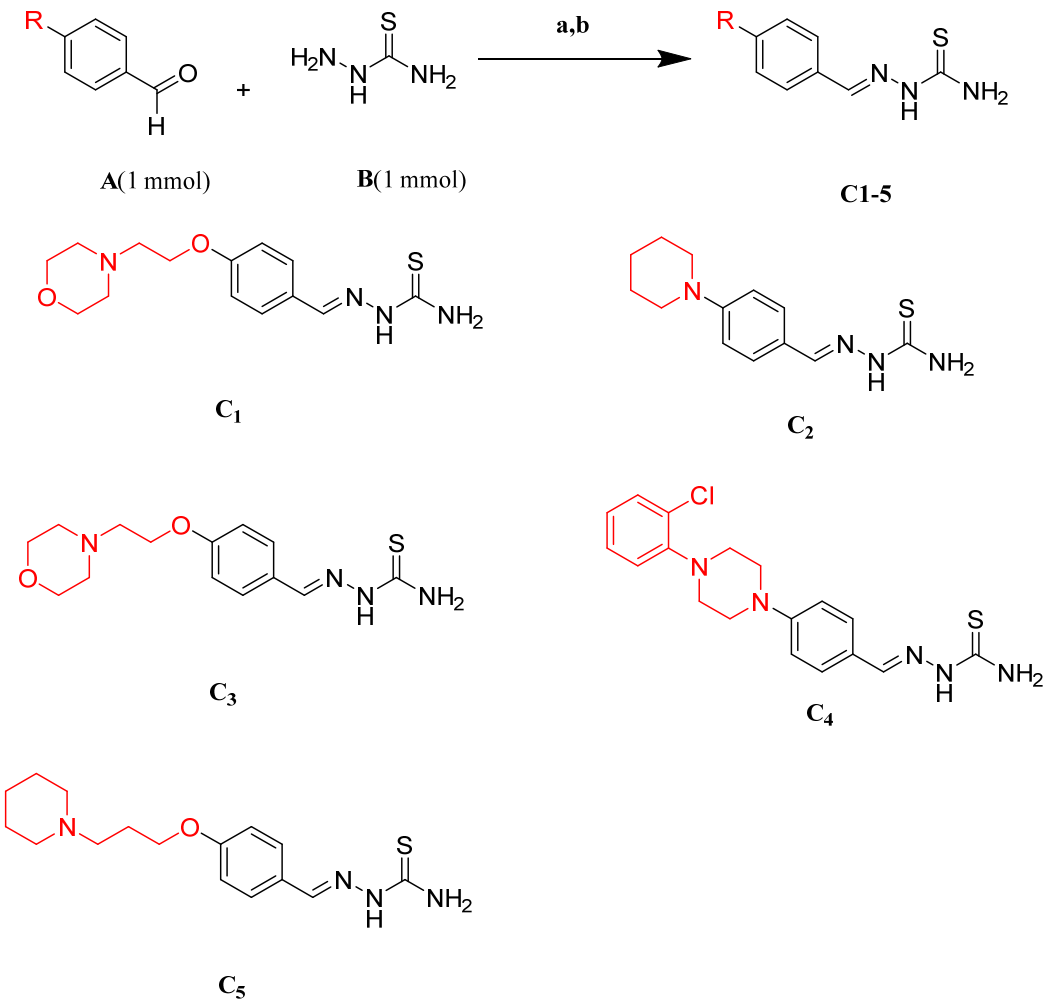

Fig. 1. Synthetic process for the thiosemicarbazone derivatives, compounds 1 to 5 (C1, C2, C3, C4, and C5). A, Benzaldehydes; B, thiosemicarbazide; a, EtOH, K_2CO_3 at room temperature, overnight; b, reflux, 1 h.

Cell viability assay

The 3-(4,5-dimethylthiazol-2-yl)-2,5-diphenyltetrazolium bromide (MTT) assay was used to evaluate the cytotoxic effects of the compounds. This colorimetric assay assesses cellular metabolic activity by measuring the ability of NADH-dependent cellular oxidoreductase enzymes to reduce MTT to its insoluble formazan, which exhibits a purple color. Initially, PC12 cells were seeded in 96-well plates at a density of 1.0×10^4 cells in each well. After 24 h incubation, the cells were exposed to various concentrations of the compounds (100-800 µM) or were left untreated (control) with only DMEM/MEM for an additional 24 h of incubation. After treatment, 20 µL of MTT reagent (5 mg/mL in phosphate-buffered saline (PBS)) was added, and the plates were incubated for 3 h at 37 °C in a 5% CO_2 atmosphere. The resulting purple formazan was dissolved in DMSO (200 µL per well), and the absorbance was measured at 570 nm using a microplate spectrophotometer (MultiSkan™, Thermo Fisher, USA). The experiments were conducted in triplicate with four parallel wells. Cell viability, expressed as a percentage relative to the untreated cells, was used to determine the concentration of each treatment that inhibited 50% of cell viability (IC_{50}), reported in µM using a dose-response curve (35,36).

Intracellular ROS generation assay

Intracellular ROS levels were evaluated by measuring the oxidation of 2′,7′-dichlorfluorescein diacetate (DCFH-DA), a non-polar, non-fluorescent compound that readily penetrates cell membranes. Once inside the cell, DCFH-DA is hydrolyzed by intracellular esterases to form DCFH, which subsequently reacts with ROS to produce the highly fluorescent DCF. For the assay, PC12 cells (2.5×10^5 cells/well) were plated in 96-well plates and allowed to adhere overnight. The culture medium was replaced with pre-warmed PBS containing 10 µM DCFH-DA. The cells were then incubated at 37 °C in the dark for 30 min to facilitate DCFH-DA uptake and conversion. After incubation, excess DCFH-DA was removed by washing the cells twice with PBS. The cells were subsequently treated with the test compounds at their IC_{50} and 1/2 IC_{50} concentrations, as determined by MTT assay and incubated for an additional 3 h at 37 °C. Fluorescence intensity was measured continuously for 30 min using a microplate spectrofluorometer, with excitation at 488 nm and emission at 525 nm. The results were expressed as a fold increase in fluorescence intensity relative to the control group (37).

GPX activity assay

GPX is an essential enzyme found in both cytoplasmic and mitochondrial compartments that catalyzes the reduction of hydrogen peroxide (H_2O_2) and lipid hydroperoxides (LOOHs), utilizing reduced glutathione (GSH) as a substrate and converting it to oxidized glutathione (GSSG). The activity of GPX can be indirectly quantified by measuring the consumption of NADPH, which is reduced to $NADP^+$ in the presence of GSH reductase during the enzymatic reaction. To evaluate GPX activity, the amount of NADPH consumed was measured. In this study, following treatment with compounds at their IC_{50} and 1/2 IC_{50} concentrations, PC12 cells (2×10^6 cells) were harvested and washed with cold PBS to remove any residual culture medium. The cell pellets were resuspended in the provided lysis buffer from the Nagpix glutathione peroxidase activity assay kit and subjected to a freeze-thaw cycle to ensure complete lysis. The assay was performed according to the manufacturer's instructions. GPX activity was quantified by measuring the decrease in absorbance at 340 nm using a microplate spectrophotometer (MultiSkan™, Thermo Fisher, USA) due to NADPH consumption, expressed as nmol NADPH consumed per min per mg of protein. Total protein content was determined using a protein assay (Bradford method) to normalize the GPX activity results.

LPO assay

The thiobarbituric acid (TBA) reactive substance assay quantifies the level of malondialdehyde (MDA), the end product of LPO. Briefly, 200 µL of the samples was combined with 1 µL of 20% trichloroacetic acid solution and allowed to stand at room temperature for 10 min. Following centrifugation at 4100 rpm for 13 min, the supernatant was

discarded. Subsequently, 800 µL of a 0.2% solution of TBA in 2 M sodium sulfate was added to the remaining sediment, vortexed to ensure dissolution, and incubated in a boiling water bath for 30 min to facilitate the reaction between MDA and TBA. After cooling to room temperature, 800 µL of n-butanol was added to extract the colored complex. The absorbance of the n-butanol phase (300 µL) was measured at 532 nm using a microplate spectrophotometer (MultiSkan™, Thermo Fisher, USA) after further centrifugation for 13 min at 4100 rpm. The concentration of MDA was calculated based on the MDA standard curve and expressed as mmol MDA/mg protein (38).

Total antioxidant capacity assay

The ferric ion-reducing antioxidant power (FRAP) assay was employed to evaluate total antioxidant capacity (TAC) by measuring the capability of samples to reduce Fe^{3+} to Fe^{2+}. In a standard procedure, 295 µL of FRAP solution, which contained acetate buffer (300 mM), ferric chloride (20 mM), and 2,4,6-tris (2-pyridyl)-s-triazine (TPTZ, 10 mM), was added to each well and incubated at 37 °C for 5 min. Subsequently, 5 µL of the plasma sample was added to each well. The microplate was then incubated at 37 °C for an additional 10 min, and the absorbance was measured at 593 nm using a microplate spectrophotometer (MultiSkan™, Thermo Fisher, USA). The total antioxidant capacity of the sample was determined in µmol Fe(II)/mg protein using the ferrous sulfate standard curve (38).

Statistical analysis

Data were presented as mean ± SD and analyzed by Graphpad Prism™ software through one-way analysis of variance (ANOVA) followed by Dunnett's post-hoc tests and dose-response analysis. *P*-values less than 0.05 are considered statistically significant.

RESULTS

Physicochemical properties of synthesized compounds

The final compounds were synthesized according to the procedure shown in Fig. 1. The condensation reaction between thiosemicarbazide and various substituted benzaldehydes yielded the corresponding target benzylidene thiosemicarbazone derivatives. The inventory, including the structures, melting points, and yields for each compound, is presented in Table 1.

The effect of the synthesized compounds on cell viability

The cytotoxic effect of compounds C1-C5 is depicted in Fig. 2. As illustrated in Fig. 2B, C2 showed the most significant cytotoxic effect in the MTT assay, with an IC_{50} of 156.2 ± 97.5 µM, whereas C4 (Fig. 2D) exhibited the lowest cytotoxicity effect with an IC_{50} of 629.7 ± 109.2 µM.

The effect of the synthesized compounds on intracellular ROS generation

The ROS generation assay was evaluated after exposing PC12 cells to the compounds at two IC_{50} and 1/2 IC_{50} concentrations. As shown in Fig. 3, the ROS production at IC_{50} concentrations for all compounds was nearly twofold compared to the control group, with no significant difference between compounds in ROS generation. However, at 1/2 IC_{50} concentrations, the ROS production rate decreased, and C3 showed the lowest ROS production compared to all other compounds.

The effect of the synthesized compounds on GPX activity

The level of GPX activity in cells exposed to all derivatives, except for C3, at 1/2 IC_{50}, decreased significantly compared to the control group (Fig. 4A).

The effect of the synthesized compounds on LPO

As shown in Fig. 4B, at 1/2 IC_{50} concentrations, all compounds significantly reduced the level of LPO compared to the control group. Additionally, C4 exhibited the most significant reduction, while C5 demonstrated the least reduction in the level of LPO compared to the control group.

The effect of the synthesized compounds on TAC

Compounds C1, C3, and C4 at 1/2 IC_{50} concentrations increased TAC compared to the control group, while C2 and C5 did not show a significant difference in TAC at 1/2 IC_{50} concentrations compared to the control group (Fig. 4C).

Table 1. The physicochemical properties of the synthesized thiosemicarbazone derivatives studied using IR, 1H NMR, and 13C NMR.

Synthesized compounds	Physicochemical properties	Yield (%)	Melting point (°C)
Compound 1 (C1): 2-(4-(2-(piperidin-1-yl)ethoxy) benzylidene) hydrazine-1-carbothioamide	IR (KBr) (ν_{max}, cm^{-1}): 3424, 3264, 3151 (CHsp2), 2853 (CHsp3), 2790 (CHsp3), 2794 (CHsp3), 1508 (C=N), 1249 (C=S), 1170 (C-O). ^{1}H NMR (300 MHz, DMDO-d_6) δ (ppm): 11.33 (1H, s, NH), 8.12 (1H, s, NH), 8.01 (H, s, CH), 7.93 (H, s, NH), 7.74 (2H, d, *J* = 9 Hz, 2CHAr), 6.98 (2H, d, *J* = 9 Hz, 2CHAr), 4.11 (2H, t, *J* = 6 Hz, OCH_2), 2.66 (2H, t, *J* = 6 Hz, NCH_2), 2.43 (4H, t, *J* = 6 Hz, CH_2NCH_2), 1.5 (4H, quint, *J* = 6 Hz, CH_2), 1.40 (2H, t, *J* = 6 Hz, CH_2). ^{13}C NMR (75 MHz, DMDO-d_6) δ (ppm): 178.1, 160.4, 142.9, 129.4, 127.2, 115.2, 66.2, 57.8, 54.9, 26.1, and 24.4.	90	172-173
Compound 1 (C2): 2-(4-(piperidin-1-yl) benzylidene) hydrazine-1-carbothioamide	IR (KBr) (ν_{max}, cm^{-1}): 3432, 3265, 3149, 2935 (CHsp2), 2853 (CHsp3), 2851 (CHsp3), 2823 (CHsp3), 1604 (C=N), 1233 (C=S).	95	169-173
Compound 1 (C3): 2-(4-(2-morpholinoethoxy) benzylidene) hydrazine-1-carbothioamide	IR (KBr) (ν_{max}, cm^{-1}): 3424, 3276, 3162, 1523 (C=N), 1273 (C=S), 1113 (C-O). ^{1}H NMR (300 MHz, DMSO-d_6) δ (ppm): 10.48 (1H, brs, NH), 7.96 (1H, s, CH), 7.32-6.91 (6H, m, CHAr and NH_2), 4.17 (2H, brs, CH_2-O), 3.77(4H, brs, $2CH_2O$, 2.85(2H, brs, CH_2N), 2.63 (4H, brs, $2CH_2N$).	97	187-189
Compound 1 (C4): 2-(4-(4-(2-chlorophenyl) piperazin-1-yl)benzylidene) hydrazine-1-carbothioamide	IR (KBr) (ν_{max}, cm^{-1}): 3421, 3324, and 3298 (NH), 1510 (C=N), 1283 (C=S), 945.91(C-Cl). ^{1}H NMR (300 MHz, DMSO-d_6) δ (ppm): 11.28 (1H, brs, NH), 8.09 (1H, brs, NH), 7.99 (1H, brs, NH), 7.88 (1H, brs, NH), 7.69 (2H, , d, *J*= 9Hz, 2CHAr), 7.47 (1H, d, *J* = 6Hz, CHAr), 7.34 (1H, d, *J* = 6Hz, CHAr), 7.23 (1H, d,*J*= 6Hz, CHAr), 7.12 (1H , d, *J* = 9Hz, CHAr), 7.05 (2H, , d, *J* = 9Hz, CHAr), 4.14(4H, brs,NCH_2), 3.62(4H, brs, NCH_2). ^{13}C NMR (75MHz, DMSO-d_6) δ (ppm): 177.78 (C=S), 152.28, 149.21, 143.20, 130.86, 129.02, 128.64, 128.13, 124.91, 124.63, 121.39, 115.21, 51.15, and 48.18(CH_2).	86	202-205
Compound 1 (C5): 2-(4-(3-(piperidin-1-yl)propoxy) benzylidene) hydrazine-1-carbothioamide	^{1}H NMR (300 MHz, DMSO-d_6) δ (ppm): 11.33 (1H, s, NH), 8.13 (H, s, NH), 8.02 (1H, s, NH), 7.92 (1H, s, CH), 7.73 (2H, d, *J* = 9 Hz, 2CHAr), 6.97 (2H, d, *J* = 9 Hz, 2CHAr), 4.04 (2H, t, *J* = 6 Hz, OCH_2), 2.39 (2H, t, *J* = 6 Hz, CH_2), 2.34 (2H, t, CH_2), 1.87 (2H, quint, *J* = 6 Hz, CH_2), 1.52-1.39 (6H, m, $3CH_2$). ^{13}C NMR (75 MHz, DMSO-d_6) δ (ppm): 178.0, 160.5, 142.7, 129.3, 127.1, 115.0, 66.5, 55.5, 54.5, 26.6, 26.0, and 24.6.	92	192-195

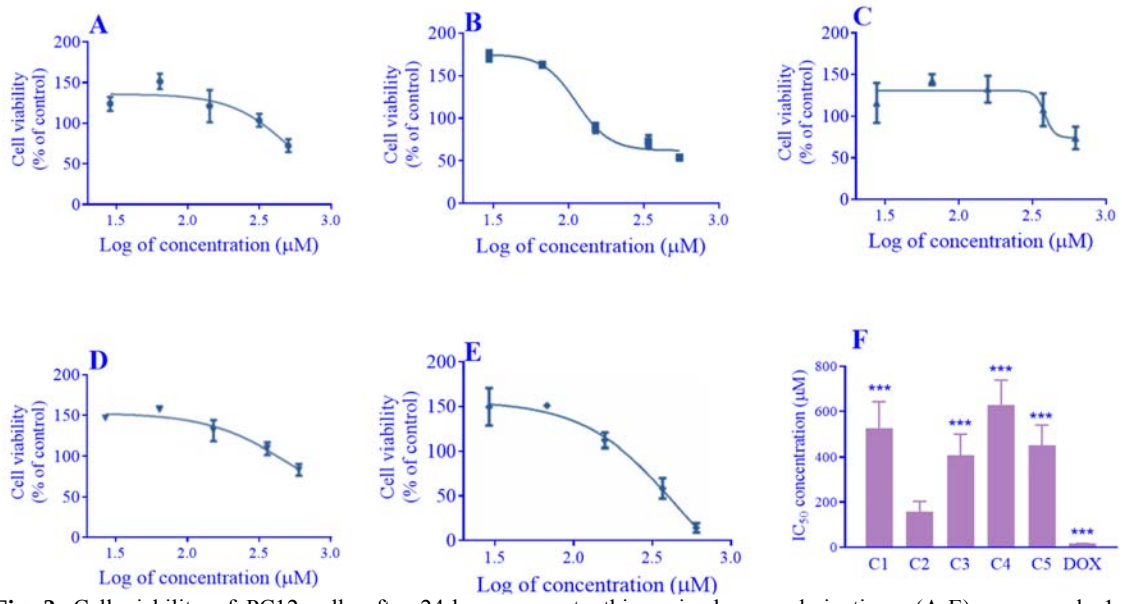

Fig. 2. Cell viability of PC12 cells after 24-h exposure to thiosemicarbazone derivatives, (A-E) compounds 1-5, respectively, using the dose-response analysis method. ((F) Bar chart represents the calculated IC_{50} for compounds 1 to 5 (C1, C2, C3, C4, and C5) and doxorubicin. Data are presented as mean ± SD of three experiments. ***$P < 0.001$ indicates significant differences compared to the C2-treated cells.

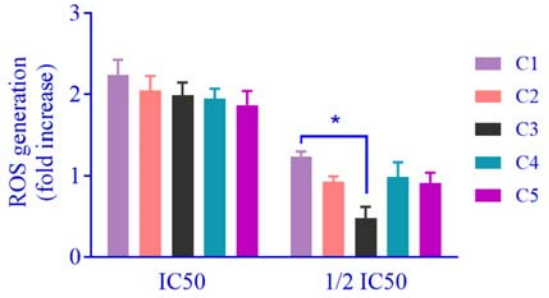

Fig. 3. The results of ROS generation in PC12 cells treated with thiosemicarbazone derivatives, compounds 1 to 5 (C1, C2, C3, C4, and C5). The ROS levels relative fluorescence units (RFU) per minute were expressed as a fold increase compared to the control group. Data are presented as mean ± SD of three experiments. *$P < 0.05$ indicates a significant difference between the designated groups.

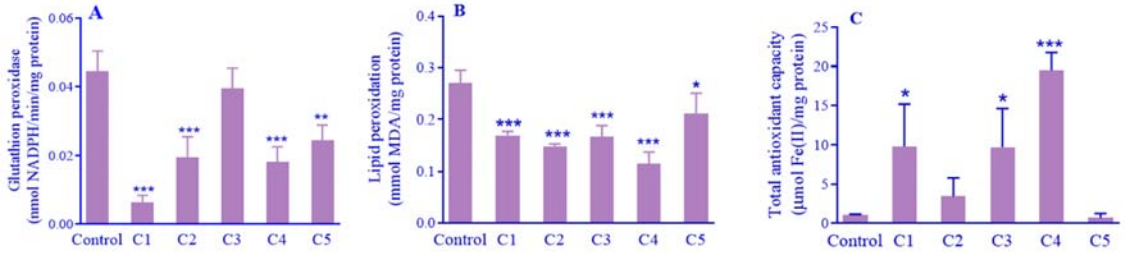

Fig. 4. The results of (A) glutathione peroxidase activity, (B) lipid peroxidation, and (C) total antioxidant capacity in PC12 cells treated with thiosemicarbazone derivatives, compounds 1 to 5 (C1, C2, C3, C4, and C5), at 1/2 IC_{50} concentrations. Data are presented as mean ± standard deviation of three experiments. *$P < 0.05$, **$P < 0.01$, and ***$P < 0.001$ indicate significant differences in comparison with the control group.

DISCUSSION

The objective of our research was to investigate the cytotoxic effects of newly synthesized thiosemicarbazone derivatives, with a specific emphasis on biomarkers of ferroptosis, a type of programmed cell death regulated by lipid-based ROS (39). Five derivatives were synthesized and characterized through IR and H/C NMR spectroscopy. Among all the synthesized compounds, C3 (2-(4-(2-morpholinoethoxy) benzylidene) hydrazine-1-carbothioamide) exhibited the most biomarkers indicative of a higher likelihood to contribute to the ferroptosis pathway. This includes the reduction of intracellular ROS production, maintained GPX activity, and an elevation in TAC. The significant reduction in ROS production at half the IC_{50} concentration reflects the dose-dependent scavenging activity of thiosemicarbazone derivatives, as reported in previous studies (40,41). C3, with the lowest ROS levels, likely owes its radical-scavenging properties to its morpholinoethoxy group, which may enhance both enzymatic and non-enzymatic antioxidant defenses. Impairments in antioxidant mechanisms, including the cystine-glutamate antiporter system Xc− and GPX4, along with dysregulated iron metabolism, contribute to ROS accumulation and ferroptotic cell death (42,43).

C2 (2-(4-(piperidin-1-yl) benzylidene) hydrazine-1-carbothioamide) showed the most pronounced cytotoxic effect in cell viability assessments *via* the MTT assay, possibly due to its enhanced solubility in water and smaller molecular weight and size, facilitating greater interaction with cellular components and more permeability. Conversely, C4 (2-(4-(4-(2-chlorophenyl) piperazin-1-yl)benzylidene) hydrazine-1-carbothioamide) exhibited reduced cytotoxicity, which might be attributed to its lower solubility in water and larger molecular weight and size, limiting its interaction with cells and permeability.

Interestingly, all the synthesized compounds except for C3 decreased GPX activity, thus promoting ferroptosis pathways. GPX enzymes are crucial in defending against oxidative damage by reducing H_2O_2 and LOOHs. The overproduction of ROS, coupled with the decline in GPX activity and the induction of LPO, suggests the potential for ferroptosis initiation in the cells treated with these compounds (44-46).

C4 exhibited the highest increase in TAC without altering LPO, possibly due to the presence of the chlorophenyl-piperazinyl moiety, which might enhance its antioxidant potential without inducing lipid damage. On the other hand, C5 (2-(4-(3-(piperidin-1-yl)propoxy)benzylidene) hydrazine-1-carbothioamide) showed the least reduction in LPO and no significant changes in TAC, suggesting weaker interaction with antioxidant mechanisms, potentially due to the propoxy-piperidinyl structure (40,47).

The diverse effects observed on ferroptosis biomarkers across the synthesized compounds can be directly attributed to their unique chemical structures, each of which influences their interaction with both enzymatic and non-enzymatic antioxidants. These structural differences influence critical factors such as lipophilicity, electronic properties, and steric hindrance that affect the compounds' ability to penetrate lipid membranes, interact with cellular macromolecules, and modulate ferroptotic pathways. C1 (2-(4-(2-(piperidin-1-yl)ethoxy)benzylidene)hydrazine-1-carbothioamide) demonstrated a significant increase in TAC, likely due to the enhanced lipophilicity conferred by the piperidinyl-ethoxy group. This structural characteristic facilitates membrane penetration and interaction with lipid components, potentially stabilizing free radicals and enhancing their antioxidant activity. Additionally, the flexibility of the alkoxy chain may further improve its radical scavenging capabilities. C2 (2-(4-(piperidin-1-yl)benzylidene)hydrazine-1-carbothioamide) exhibited the most significant cytotoxic effect, likely due to its simpler structure, which lacks an alkoxy chain. This structural simplicity increases solubility, thereby enhancing cellular uptake and interaction. The improved solubility contributes to the reduction of GPX activity and induces oxidative stress, which promotes ferroptosis.

Furthermore, the direct interaction with cellular components likely amplifies its capacity to trigger ferroptosis through these mechanisms. C3 (2-(4-(2-morpholinoethoxy)benzylidene) hydrazine-1-carbothioamide) was distinguished by its lowest ROS production and maintained GPX activity, indicative of potent antioxidant properties. The morpholino group in its structure enhances hydrophilicity and electron-donating capacity, thereby improving its interaction with both enzymatic and non-enzymatic antioxidant systems. This enhancement contributes to its superior ability to scavenge free radicals, likely accounting for its protective effects against ferroptosis. The bulky chlorophenyl-piperazinyl group introduces steric hindrance, possibly reducing its solubility and cytotoxicity. However, the chlorophenyl ring can stabilize free radicals, enhancing antioxidant effects. This structural feature likely aids in protecting against oxidative damage without significantly inducing ferroptosis. C5 (2-(4-(3-(piperidin-1-yl)propoxy) benzylidene) hydrazine-1-carbothioamide) exhibited minimal reduction in LPO and did not significantly alter TAC. The longer propoxy chain in C5 may diminish its capacity to interact with antioxidant systems or disrupt lipid membranes as effectively as the other compounds, which contributes to its limited impact on ferroptosis biomarkers. This reduced interaction with cellular defense mechanisms underscores the significance of chain length and flexibility in influencing biological activity. Overall, the structural variations among these compounds significantly affect their biological activity and potential to modulate ferroptosis. These differences highlight the critical of functional groups in determining their interactions with cellular antioxidant defenses and their ability to induce or prevent ferroptotic cell death. Understanding these structure-activity relationships is essential for optimizing the design of ferroptosis-inducing agents or antioxidants targeting this pathway.

CONCLUSION

In conclusion, the five bioactive thiosemicarbazone derivatives synthesized through a condensation reaction between thiosemicarbazide and the synthesized benzaldehyde enhanced the antioxidant capacity of cells and reduced oxidative damage to cellular lipids. Given the potential chelation properties of these compounds, they may contribute to the ferroptosis cell death pathway. Therefore, further studies are needed to evaluate the ability of these compounds to bind to iron, a key element in the induction of ferroptosis.

Acknowledgments

The authors would like to acknowledge the financial support of the Kerman University of Medical Sciences (KMU) Research Vice-Chancellor for this project (Reg. No. 401000340 and ethical approval: IR.KMU.REC.1401.403).

Conflict of interest statement

The authors declared no conflict of interest in this study.

Authors' contributions

Y. Pourshojaei and S. Karami-Mohajeri had the idea for the article and critically revised the work. Y. Shadmani performed the literature search and synthesized and tested compounds. M. Sadeghzadeh synthesized and performed the spectral analysis. Y. Shadmani and B. Amirheidari drafted the work. The finalized article was read and approved by all authors.

REFERENCES

1. Napotnik TB, Polajžer T, Miklavčič D. Cell death due to electroporation - a review. Bioelectrochemistry. 2021;141:107871. DOI: 10.1016/j.bioelechem.2021.107871.
2. Kopeina GS, Zhivotovsky B. Programmed cell death: past, present and future. Biochem Biophys Res Commun. 2022;633:55-58. DOI: 10.1016/j.bbrc.2022.09.022.
3. Lockshin RA, Williams CM. Programmed cell death, cytology of degeneration in the intersegmental muscles of the *Pernyi silkmoth*. J Insect Physiol.1965;11(2):123-133. DOI: 10.1016/0022-1910(65)90099-5.
4. Kerr JFR, Wyllie AH, Currie AR. Apoptosis: a basic biological phenomenon with wide-ranging implications in tissue kinetics Br J Cancer.. 1972;26(4):239-257. DOI: 10.1038%2Fbjc.1972.33.

5. Galluzzi L, Vitale I, Aaronson SA, Abrams JM, Adam D, Agostinis P, *et al*. Molecular mechanisms of cell death: recommendations of the Nomenclature Committee on Cell Death 2018. Cell Death Differ. 2018;25(3):486-541. DOI: 10.1038/s41418-017-0012-4.
6. Henke N, Albrecht P, Bouchachia I, Ryazantseva M, Knoll K, Lewerenz J, *et al*. The plasma membrane channel ORAI1 mediates detrimental calcium influx caused by endogenous oxidative stress. Cell Death Dis. 2013;4(1):e470,1-9. DOI: 10.1038/cddis.2012.216.
7. Dixon Scott J, Lemberg Kathryn M, Lamprecht Michael R, Skouta R, Zaitsev Eleina M, Gleason Caroline E, *et al*. Ferroptosis: an iron-dependent form of nonapoptotic cell death. Cell. 2012;149(5):1060-1072. DOI: 10.1016/j.cell.2012.03.042.
8. Stockwell BR, Jiang X, Gu W. Emerging mechanisms and disease relevance of ferroptosis. Trends Cell Biol. 2020;30(6):478-490. DOI: 10.1016/j.tcb.2020.02.009.
9. Jiang X, Stockwell BR, Conrad M. Ferroptosis: Mechanisms, biology and role in disease. Nat Rev Mol Cell Biol. 2021;22(4):266-282. DOI: 10.1038/s41580-020-00324-8.
10. Han C, Liu Y, Dai R, Ismail N, Su W, Li B. Ferroptosis and its potential role in human diseases. Front Pharmacol. 2020;11:239,1-19. DOI: 10.3389/fphar.2020.00239.
11. Zhang Y, Xin L, Xiang M, Shang C, Wang Y, Wang Y, *et al*. The molecular mechanisms of ferroptosis and its role in cardiovascular disease. Biomed Pharmacother. 2022;145:112423. DOI: 10.1016/j.biopha.2021.112423
12. Huang F, Yang R, Xiao Z, Xie Y, Lin X, Zhu P, *et al*. Targeting ferroptosis to treat cardiovascular diseases: a new continent to be explored. Front Cell Dev Biol. 2021;9:737971. DOI: 10.3389/fcell.2021.737971.
13. Nakamura T, Naguro I, Ichijo H. Iron homeostasis and iron-regulated ROS in cell death, senescence and human diseases. Biochim Biophys Acta Gen Subj. 2019;1863(9):1398-1409. DOI: 10.1016/j.bbagen.2019.06.010.
14. Wu S, Li T, Liu W, Huang Y. Ferroptosis and cancer: complex relationship and potential application of exosomes. Front Cell Dev Biol. 2021;9:733751. DOI: 10.3389/fcell.2021.733751.
15. Shintoku R, Takigawa Y, Yamada K, Kubota C, Yoshimoto Y, Takeuchi T, *et al*. Lipoxygenase-mediated generation of lipid peroxides enhances ferroptosis induced by erastin and RSL3. Cancer Sci. 2017;108(11):2187-2194. DOI: 10.1111/cas.13380.
16. Yan B, Ai Y, Sun Q, Ma Y, Cao Y, Wang J, et al. Membrane damage during ferroptosis is caused by oxidation of phospholipids catalyzed by the oxidoreductases POR and CYB5R1. Mol Cell. 2021;81(2):355-69.e10. DOI: 10.1016/j.molcel.2020.11.024.
17. Lee JY, Kim WK, Bae KH, Lee SC, Lee EW. Lipid metabolism and ferroptosis. Biology. 2021;10(3):184,1-16. DOI: 10.3390/biology10030184.
18. Li S, Zhang X. Iron in cardiovascular disease: challenges and potentials. Front Cardiovasc Med. 2021;8:707138. DOI: 10.3389/fcvm.2021.707138.
19. Weber S, Parmon A, Kurrle N, Schnütgen F, Serve H. The clinical significance of iron overload and iron metabolism in myelodysplastic syndrome and acute myeloid leukemia. Front Immunol. 2021;11:627662. DOI: 10.3389/fimmu.2020.627662.
20. Yan HF, Zou T, Tuo QZ, Xu S, Li H, Belaidi AA, *et al*. Ferroptosis: mechanisms and links with diseases. Signal Transduction Targeted Ther. 2021;6(1):49. DOI: 10.1038/s41392-020-00428-9.
21. Jakaria M, Belaidi AA, Bush AI, Ayton S. Ferroptosis as a mechanism of neurodegeneration in Alzheimer's disease. J Neurochem. 2021;159(5):804-825. DOI: 10.1111/jnc.15519.
22. Yiannikourides A, Latunde-Dada GO. A short review of iron metabolism and pathophysiology of iron disorders Medicines. 2019;6(3):85. DOI: 10.3390/medicines6030085.
23. Anderson GJ, Frazer DM. Current understanding of iron homeostasis. Am J Clin Nutr. 2017;106(Suppl 6):1559S-1566S. DOI: 10.3945/ajcn.117.155804.
24. Salimi A, Sharif Makhmal Zadeh B, Kazemi M. Preparation and optimization of polymeric micelles as an oral drug delivery system for deferoxamine mesylate: *in vitro* and *ex vivo* studies. Res Pharm Sci. 2019;14(4):293-307. DOI: 10.4103/1735-5362.263554.
25. Kruszewski M. Labile iron pool: the main determinant of cellular response to oxidative stress. Mutat Res. 2003;531(1-2):81-92. DOI: 10.1016/j.mrfmmm.2003.08.004.
26. Yin H, Xu L, Porter NA. Free radical lipid peroxidation: mechanisms and analysis. Chem Rev. 2011;111(10):5944-5972. DOI: 10.1021/cr200084z.
27. Zilka O, Shah R, Li B, Friedmann Angeli JP, Griesser M, Conrad M, Pratt DA. On the mechanism of cytoprotection by ferrostatin-1 and liproxstatin-1 and the role of lipid peroxidation in ferroptotic cell death. ACS Cent Sci. 2017;3(3):232-243. DOI: 10.1021/acscentsci.7b00028.
28. Ratan RR. The chemical biology of ferroptosis in the central nervous system. Cell Chem Biol. 2020;27(5):479-498. DOI: 10.1016/j.chembiol.2020.03.007.
29. Zhang J, Zhao H, Yao G, Qiao P, Li L, Wu S. Therapeutic potential of iron chelators on osteoporosis and their cellular mechanisms. Biomed Pharmacother. 2021;137:111380. DOI: 10.1016/j.biopha.2021.111380.
30. Richardson DR, Kalinowski DS, Lau S, Jansson PJ, Lovejoy DB. Cancer cell iron metabolism and the development of potent iron chelators as anti-tumour

agents. Biochim Biophys Acta Gen Subj.. 2009;1790(7):702-717.
DOI: 10.1016/j.bbagen.2008.04.003.
31. Kaplancıklı ZA, Altıntop MD, Sever B, Cantürk Z, Özdemir A. Synthesis and *in vitro* evaluation of new thiosemicarbazone derivatives as potential antimicrobial agents. Chinese J Chem. 2016;2016:1692540,1-7.
DOI: 10.1155/2016/1692540.
32. Shahlaei M, Fassihi A, Nezami A. QSAR study of some 5-methyl/trifluoromethoxy- 1H-indole-2,3-dione-3-thiosemicarbazone derivatives as anti-tubercular agents. Res Pharm Sci. 2009;4(2):123-131.
PMID: 21589807.
33. Hassan M, Ghaffari R, Sardari S, Farahani YF, Mohebbi S. Discovery of novel isatin-based thiosemicarbazones: synthesis, antibacterial, antifungal, and antimycobacterial screening. Res Pharm Sci. 2020;15(3):281-290.
DOI: 10.4103/1735-5362.288435.
34. Eslaminejad T, Pourshojaei Y, Naghizadeh M, Eslami H, Daneshpajouh M, Hassanzadeh A. Synthesis of some benzylidene thiosemicarbazide derivatives and evaluation of their cytotoxicity on U87, MCF-7, A549, 3T3 and HUVEC cell lines: scientific paper. J Serbian Chem Soc. 2022;87(10):1125-1142.
DOI: 10.2298/JSC210630016E.
35. Soltani M, Karami-Mohajeri S, Ranjbar M, Ahmadi N, Jafari E, Mandegari A, *et al*. Reducing the cytotoxicity of magnesium oxide nanoparticles using cerium oxide shell coating: an *in vitro* and *in vivo* study. Ceram Int. 2023;49(9):14733-14743.
DOI: 10.1016/j.ceramint.2023.01.069.
36. Manmuan S, Tubtimsri S, Chaothanaphat N, Issaro N, Tantisira MH, Manmuan P. Determination of the anticancer activity of standardized extract of *Centella asiatica* (ECa 233) on cell growth and metastatic behavior in oral cancer cells. Res Pharm Sci. 2024;19(2):121-147.
DOI: 10.4103/rps.rps_81_23.
37. Sinaei N, Mirakabadi A, Jafari E, Karami-Mohajeri S. The cytotoxic effects of partially purified cytotoxic peptides of *Naja naja* Oxiana venom on human glioblastoma multiforme: an *in vitro* study. Int J Pept Res Ther. 2022;29,14.
DOI: 10.1007/s10989-022-10479-x.
38. Ahmadipour A, Sharififar F, Pournamdari M, Mandegary A, Hosseini A, Afrapoli FM, *et al*. Hepatoprotective effect of *Zataria multiflora* Boiss against malathion-induced oxidative stress in male rats. Orient Pharm Exp Med. 2016;16(4): 287-293.
DOI: 10.1007/s13596-016-0238-6.
39. Cheng Y, Song Y, Chen H, Li Q, Gao Y, Lu G, Luo C. Ferroptosis mediated by lipid reactive oxygen species: a possible causal link of neuroinflammation to neurological disorders. Oxid Med Cell Longev. 2021;2021:5005136.
DOI: 10.1155/2021/5005136.
40. Qi F, Qi Q, Song J, Huang J. Synthesis, crystal structure, biological evaluation and *in silico* studies on novel (e)-1-(substituted benzylidene)-4-(3-isopropylphenyl)thiosemicarbazone derivatives. Chem Biodivers. 2021;18(2):e2000804,1-13.
DOI: 10.1002/cbdv.202000804.
41. Finkel T. Signal transduction by reactive oxygen species. J Cell Biol. 2011;194(1):7-15.
DOI: 10.1083/jcb.201102095.
42. Yang WS, SriRamaratnam R, Welsch ME, Shimada K, Skouta R, Viswanathan VS, *et al*. Regulation of ferroptotic cancer cell death by gpx4 Cell. 2014;156(1-2):317-331.
DOI: 10.1016/j.cell.2013.12.010.
43. Lane DJ, Merlot AM, Huang ML, Bae DH, Jansson PJ, Sahni S, *et al*. Cellular iron uptake, trafficking and metabolism: key molecules and mechanisms and their roles in disease. Biochim Biophys Acta. 2015;1853(5):1130-1144.
DOI: 10.1016/j.bbamcr.2015.01.021.
44. Brigelius-Flohé R, Maiorino M. Glutathione peroxidases. Biochim Biophys Acta. 2013;1830(5):3289-3303.
DOI: 10.1016/j.bbagen.2012.11.020.
45. Sies H. Oxidative stress: oxidants and antioxidants. Exp Physiol.1997;82(2):291-295.
DOI: 10.1113/expphysiol. 1997. sp004024.
46. Zhong Z, Zhong Z, Xing R, Li P, Mo G. The preparation and antioxidant activity of 2-[phenylhydrazine (or hydrazine)-thiosemicarbazone]-chitosan. Int J Biol Macromol. 2010;47(2):93-97.
DOI: 10.1113/expphysiol. 1997. sp004024.
47. Yang L, Liu H, Xia D, Wang S. Antioxidant properties of camphene-based thiosemicarbazones: experimental and theoretical evaluation. Molecules. 2020;25(5):1192.
DOI: 10.3390/molecules25051192.